Porphyrin-Based Hole Conducting Electropolymer

Paul A. Liddell, Miguel Gervaldo, James W. Bridgewater, Amy E. Keirstead, Su Lin, Thomas A. Moore,* Ana L. Moore,* and Devens Gust*

Department of Chemistry and Biochemistry, Center for the Study of Early Events in Photosynthesis, Arizona State University, Tempe, Arizona 85287

Received August 14, 2007. Revised Manuscript Received November 1, 2007

The monomer 5-(4-aminophenyl)-10,20-bis(2,4,6-trimethylphenyl)porphyrin was synthesized and found to electropolymerize on platinum, indium tin oxide, and other electrodes to form a clear, semiconducting film with strong absorption in the visible spectral region. The linear, hole-conducting polymer has a unique structure, with porphyrin units linked to one another through the 5-(4-aminophenyl) nitrogen atom and the carbon atom at the 15-position on the macrocyclic ring. The porphyrin macrocyclic ring is thus an integral part of the linear polymer backbone. The oxidation potential of the film is 0.85 V and the reduction potential is −1.12 V vs SCE. The absorption spectrum of the film resembles that of a monomeric model porphyrin, but with significant peak broadening. Streak camera studies of the fluorescence of the polymer yield a lifetime of 15 ps, indicating strong quenching of the porphyrin first excited singlet state relative to that of the monomer. The properties of the polymer suggest that it may be useful in sensors, catalysts, and solar energy conversion devices.

Introduction

Porphyrins and their relatives are among the most-studied organic chromophores, not only because of their roles as biological light absorbers, redox centers, and oxygen carriers but also because of their attractive chemical properties and potential technological applications. Such applications include solar energy conversion, sensors, catalysts, biomedicine, molecular electronics, and photonics. Many of these uses require the porphyrin to convert a molecular change into an electrical signal, or vice-versa. Examples are the transduction of ligand binding by a metalloporphyrin into an electrical response that comprises the output of a sensor, or redox catalysis on an electrode surface. Another is the conversion of light energy into electrochemical potential at an electrode in a solar-energy-harvesting application. We and others have reported a large number of molecular constructs that mimic photosynthetic reaction centers by absorbing light and converting it to intramolecular electrochemical potential in the form of a charge-separated state.[1–5] A next challenge is to access this stored energy to produce electricity or fuels. This will involve the movement of electrons and oxidizing equivalents (holes) away from the molecule to electrodes or catalytic sites.

One attractive way to interface porphyrins with electrodes or catalysts is to incorporate them into electrically conducting polymers that can move electrons or holes from the site of their generation to a conductor, modulate the transport of electrons between conductors, or otherwise transduce a molecular event into an electrical response. A convenient way to produce a conducting porphyrin polymer on an electrode is to grow it there via electropolymerization. Such a method is simple and ensures good electrical conductivity across the interface. A variety of porphyrin-containing electropolymers have been reported.[6–12] In these systems, polymerization occurs via substituents attached to the porphyrin ring, rather than through the carbon atoms of the macrocyclic ring itself. Porphyrin electropolymers based on polyaniline are especially well studied.[6,7,11] The groups of Spiro and of Murray and other investigators have extensively studied the electropolymerization of 5,10,15,20-tetrakis(2-aminophenyl)porphyrins[13–19] and found that they polymerize oxidatively via the *meso*-aniline rings in a head-to-tail fashion

* Corresponding author. E-mail: gust@asu.edu.

(1) Gust, D.; Moore, T. A. Intramolecular photoinduced electron transfer reactions of porphyrins. In *The Porphyrin Handbook*, Kadish, K. M., Smith, K. M., Guilard, R., Eds.; Academic Press: New York, 2000; pp 153–190.
(2) Gust, D.; Moore, T. A.; Moore, A. L. *Acc. Chem. Res.* **2001**, *34*, 40–48.
(3) Wasielewski, M. R. *Chem. Rev.* **1992**, *92*, 435–461.
(4) Fukuzumi, S.; Imahori, H. *Electron Transfer in Chemistry*; Wiley-VCH: Weinheim, Germany, 2001; Vol. 2, pp 927–975.
(5) Guldi, D. M. *Chem. Soc. Rev.* **2002**, *31*, 22–36.
(6) Bedioui, F.; Devynck, J.; Bied-Charreton, C. *Acc. Chem. Res.* **1995**, *28*, 30–36.
(7) Fish, J. R.; Kubaszewski, E.; Peat, A.; Malinski, T.; Kaczor, J.; Kus, P.; Czuchajowski, L. *Chem. Mater.* **1992**, *4*, 795–803.
(8) Poriel, C.; Ferrand, Y.; Le Maux, P.; Paul-Roth, C.; Simonneaux, G.; Rault-Berthelot, J. *J. Electroanal. Chem.* **2005**, *583*, 92–103.
(9) Basu, J.; Rohatgimukherjee, K. K. *Solar Energy Mater.* **1991**, *21*, 317–325.
(10) Duanmu, D.-S.; Chen, Z.-P.; Yu, X.-S.; Zhou, X. *Chin. J. Chem.* **2004**, *22*, 779–781.
(11) Wohrle, D. *J. Porphyrins Phthalocyanines* **2000**, *4*, 418–424.
(12) Li, G.; Bhosale, S.; Tao, S.; Guo, R.; Bhosale, S.; Li, F.; Zhang, T.; Wang, T.; Furhop, J.-H. *Polymer* **2005**, *46*, 5299–5307.
(13) Macor, K. A.; Su, Y. O.; Miller, L. A.; Spiro, T. G. *Inorg. Chem.* **1987**, *26*, 2594–2598.
(14) Bettelheim, A.; White, B.; Raybuck, S.; Murray, R. W. *Inorg. Chem.* **1987**, *26*, 1009–1017.
(15) Bettelheim, A.; White, B. A.; Murray, R. W. *J. Electroanal. Chem.* **1987**, *217*, 271–286.
(16) Bettelheim, A.; Ozer, D.; Harth, R.; Murray, R. W. *J. Electroanal. Chem.* **1989**, *266*, 93–108.
(17) White, B. A.; Murray, R. W. *J. Electroanal. Chem.* **1985**, *189*, 345–352.
(18) Bruti, E. M.; Giannetto, M.; Mori, G.; Seeber, R. *Electroanalysis* **1999**, *11*, 565–572.

10.1021/cm7022955 CCC: $40.75
Published on Web 12/06/2007

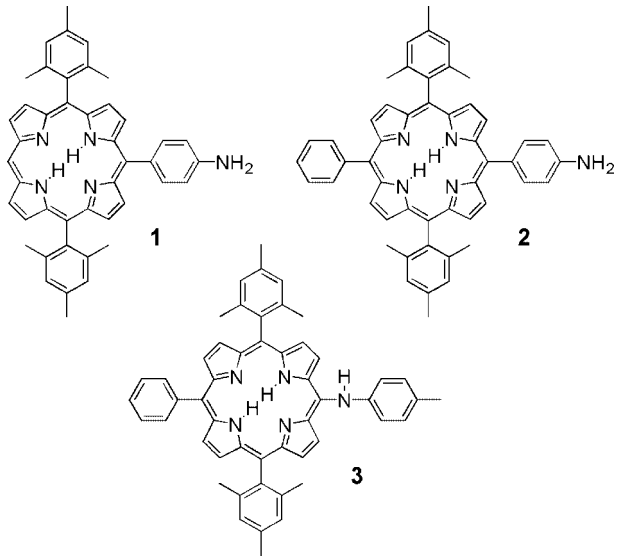

Figure 1. Structures of porphyrin monomer **1** and model compounds **2** and **3**.

in much the same way as aniline itself. Porphyrin units can bridge between the polyaniline chains. The resulting material is essentially a form of polyaniline with attached porphyrin moieties. Hole conductivity in these polymers can thus occur in ways similar to conduction in polyaniline, although the porphyrin ring could be involved in interchain hopping. Lin and co-workers reported electropolymerization of metallo-5,15-diphenyl-10-(4-aminophenylethynyl)porphyrins and concluded that polymerization of these materials also occurred in the aniline substituents, "causing minimal impact on the porphyrin π-system."[20]

Herein, we report the preparation of a new porphyrin monomer, **1** (Figure 1), and its electropolymerization to form a hole-conducting film on metal or indium tin oxide (ITO) electrodes. Polymerization occurs via bonding of the aminophenyl nitrogen directly to the carbon atom at the 15-position of the porphyrin ring. Because of this unique polymerization mechanism, the porphyrin macrocycle is an integral part of the linear, conjugated, semiconducting polymer backbone. The polymer has interesting optical and electrochemical properties that suggest it might be useful for photovoltaic and sensing applications.

Results and Discussion

Synthesis of the Monomer and Model Compounds. Monomer 5-(4-aminophenyl)-10,20-bis(2,4,6-trimethylphenyl)porphyrin, **1**, and model compounds 5-(4-aminophenyl)-10,20-bis(2,4,6-trimethylphenyl)-15-phenylporphyrin, **2**, and 5-phenylamino-10,20-bis(2,4,6-trimethylphenyl)-15-phenylporphyrin, **3**, were prepared as described in detail in the Supporting Information. Porphyrin **1** was prepared by coupling 5-bromo-10,20-bis(2,4,6-trimethylphenyl)porphyrin with a protected 4-aminophenylboronic acid derivative using a palladium complex catalyst and hydrolyzing the resulting amide derivative of **1** with acid. The amino group of the boronic acid was protected as either a *t*-butylcarbamate or an acetamido group. The former was somewhat more satisfactory.

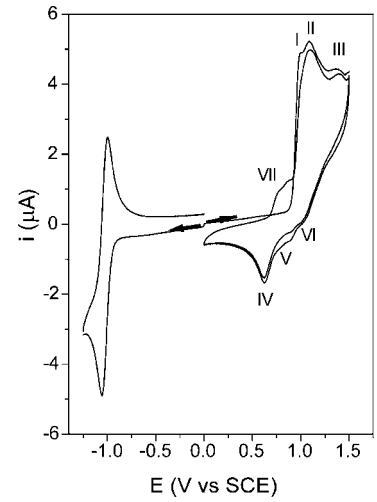

Figure 2. Cyclic voltammetry of **1** in dry, deoxygenated acetonitrile containing tetra-*n*-butylammonium hexafluorophosphate. The working and counter electrodes were platinum, and the scan rate was 0.1 V s^{-1}. The arrows indicate the initial scan directions for the anodic and cathodic sweeps. The significance of the maxima, indicated by Roman numerals, is discussed in the text.

Electrochemistry. Cyclic voltammetry (CV) of **1** in dry, deoxygenated acetonitrile containing tetra-*n*-butylammonium hexafluorophosphate supporting electrolyte was carried out using a platinum disk working electrode, a platinum counter electrode, and a Ag/AgCl quasi-reference electrode, as detailed in the Experimental Section. The scan rate was 0.1 V s^{-1}. The results are shown in Figure 2. In the cathodic scan, a reversible redox couple is observed at –1.0 V vs SCE, and a second at –1.3 V (not shown). These correspond to porphyrin ring reduction and formation of the radical anion and dianion, respectively. This is typical behavior for a phenyl-substituted porphyrin. The behavior in anodic scans is more interesting. The first positive sweep shows three oxidation waves (I, II, and III in Figure 2). There are no complementary reduction peaks in the negative sweep, showing the process to be irreversible. However, an oxidation product is detected via its reduction at 0.55 V (IV) with two shoulders (V, VI). Oxidation waves I–III occur at potentials typical for oxidation of both aryl-substituted porphyrins and aniline. The oxidation potential for aniline in acetonitrile, for example, is 0.90 V vs SCE,[21] and 5,10,15,20-tetraphenylporphyrin in benzonitrile features oxidation waves at 1.08 and 1.23 V.[22]

On the second anodic scan, a new feature (VII) appears at potentials less positive than that for peak I. Because this new feature appears only on the second scan, it must represent oxidation of the product of a chemical reaction that occurs during the initial anodic cycle. The fact that this new product is oxidized at less positive potentials than **1** suggests that it may have a more extended π-electron system than does the monomer.[23]

(19) Griveau, S.; Albin, V.; Pauporte, T.; Zagal, J. H.; Bedioui, F. *J. Mater. Chem.* **2002**, *12*, 225–232.
(20) Lin, C. Y.; Hung, Y. C.; Liu, C. M.; Lo, C. F.; Lin, Y. C.; Lin, C. L. *Dalton Trans.* **2005**, 396–401.
(21) Hand, R. L.; Nelson, R. F. *J. Am. Chem. Soc.* **1974**, *96*, 850–860.
(22) Jamin, M. E.; Iwamoto, R. T. *Inorg. Chim. Acta* **1978**, *27*, 135–143.

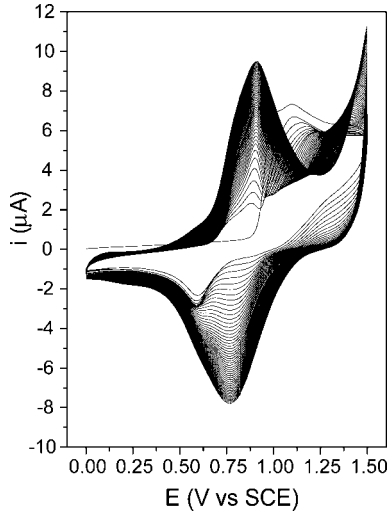

Figure 3. Cyclic voltammograms showing repetitive anodic sweeps at a platinum electrode immersed in a solution of monomer **1** as described in Figure 2. A total of 50 scans are shown. The increase in current with successive scans indicates electropolymerization.

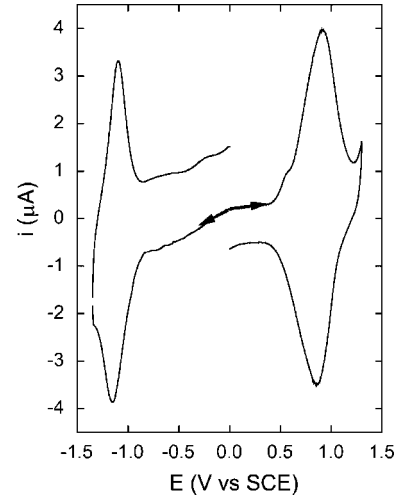

Figure 4. Cyclic voltammograms of a film of electropolymerized **1** resulting from 50 cycles under the conditions described for Figure 3. The CV conditions were the same as indicated in Figure 2, except that the electrolyte solution contained no monomer **1**. The arrows indicate the direction of the voltage sweep.

When the solution of **1** is repetitively cycled between 0.0 and 1.5 V, a new, reversible redox system continues to develop (Figure 3). The peaks observed in the first scan disappear and are replaced with a bell-shaped wave with a potential of 0.85 V. This shape is characteristic of an electrochemical process in which both oxidation and reduction are due to a species adsorbed on the electrode surface.[24] The behavior shown in Figure 3 is characteristic of electropolymerization of a monomer to form a stable hole-conducting polymer. On each successive cyclic voltammetric scan, the current increases because oxidation involves not only oxidation of the existing polymer on the electrode, but also new material from solution to form a new, thicker layer of polymer. Obviously, oxidation of the new material in solution requires electron/hole transport through the existing polymer.

When the polymer-coated Pt electrode is removed from the monomer solution, rinsed with acetonitrile, and transferred to a new solution of electrolyte containing no monomer, it shows the redox responses depicted in Figure 4. The oxidation wave is reversible, with a potential of 0.85 V, showing a nearly symmetrical current response. The separation between the anodic and cathodic peaks is near 25 mV at slow scan rates (2 mV/s), suggesting nonideal behavior.[25] The peak current is proportional to the scan rate in the range 2–500 mV/s, indicative of an irreversibly adsorbed product on the electrode. The polymer is also active in reduction, showing a reversible wave at –1.12 V with a current magnitude similar to that observed in the anodic scan.

The behavior of **1** contrasts strongly with that of model compound **2**, whose structure differs in that it has a phenyl substituent at the 15-position, rather than a hydrogen atom. In cyclic voltammetry as described above for **1**, but using a glassy carbon working electrode, the cathodic sweep for **2** yields a reversible wave with a potential of –1.25 V vs SCE. Oxidation shows three peaks at 0.92, 1.08 and 1.30 V, but these are only partially reversible, and an oxidation product is observed on the negative sweep at about 0.1 V. For **2**, with either a glassy carbon or a platinum electrode as described for **1** above, repetitive scanning from 0 to 1.5 V does not result in electropolymerization. In fact, the voltammetric response gradually decreases in amplitude after many scans. Thus, blocking of the porphyrin meso position by substitution with phenyl precludes electropolymerization. A similar lack of electropolymerization has been reported in a related compound.[7]

Electropolymerization of **1** was also carried out on transparent electrodes consisting of a thin layer of indium tin oxide (ITO) on glass in order to allow spectroscopic studies. Electrochemical behavior similar to that on Pt was seen during polymerization, with less diminution of additional current per sweep than is evident in Figure 3. The main oxidation wave is observed at ∼0.85 V vs SCE, and a second oxidation wave is observed in the anodic sweep at 1.35 V. When the electrode with the polymerized film is removed, rinsed, and placed in a cell that does not contain monomer, the resulting CV is essentially identical to that in Figure 4, with an oxidation potential of 0.85 V. Electropolymerization was also observed on gold and glassy carbon electrodes.

Spectroscopic Properties. Figure 5a shows the absorption spectra of monomer **1** and model compound **3** in dichloromethane. The spectra feature Soret bands at 414 and 421 for **1** and **3**, respectively. The Q-bands are observed at 510, 545, 585, and 641 nm for **1** and 520, ∼570, ∼590, and 664 nm for **3**. These spectra are typical for porphyrins of this type. The polymer film deposited on ITO is clear, glassy-appearing, and greenish-brown in color. Figure 5b shows spectra of films on ITO, taken in air, as a function of the number of cyclic voltammetric cycles. The spectral shape is generally similar to those of the monomer and model compound; the Soret and four Q-bands are still present. This result indicates that the basic porphyrin macrocyclic skeleton

(23) Vettorazzi, N.; Silber, J. J.; Sereno, L. *J. Electroanal. Chem.* **1981**, *125*, 459–475.
(24) Guarr, T. F.; Anson, F. C. *J. Phys. Chem.* **1987**, *91*, 4037–4043.
(25) Brown, A. P.; Anson, F. C. *Anal. Chem.* **1977**, *49*, 1589–1595.

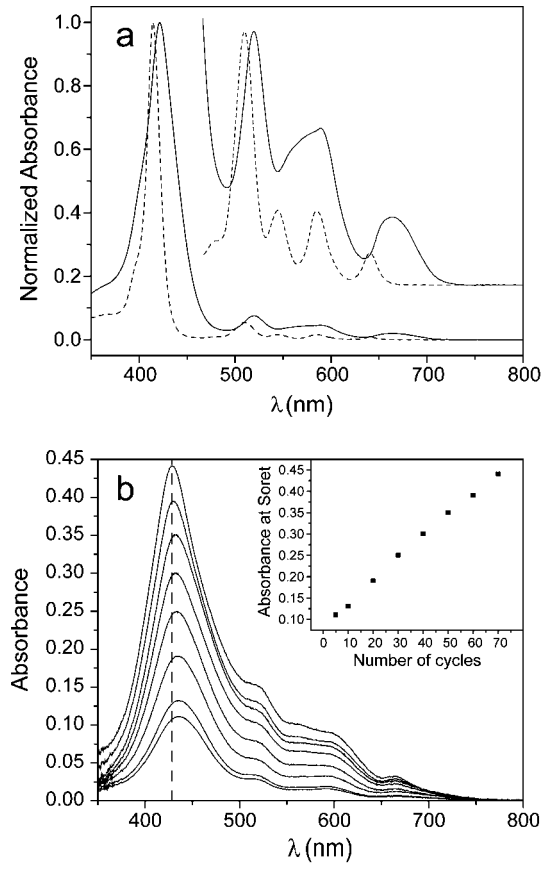

Figure 5. (a) Absorption spectra of **1** (- - - -) and **3** (——) in dichloromethane. An expansion of the Q-band region is included. (b) Absorption spectra in air of the electropolymer on ITO following 5, 10, 20, 30, 40, 50, 60, and 70 CV cycles. As emphasized by the dashed line, the Soret absorbance maximum shifts to shorter wavelengths as the number of cycles increases. The inset shows that the maximum absorbance at the Soret band increases linearly for at least the first 60–70 cycles.

is still present in the polymer. In fact, the polymer spectrum is very similar to that of model compound **3**, with the exception of spectral broadening and shifts in the maxima.

The Soret maximum of the polymer blue shifts from 436 nm after 5 cycles to 429 nm after 70 cycles, as is apparent from examining the region around the dashed line in Figure 5b. This shifting and broadening suggest that there may be $\pi-\pi$ interactions between the macrocycles in the film that change somewhat as film formation progresses. The spectrum could also be a function of polymer chain length due to electron delocalization along the backbone.

The inset in Figure 5b demonstrates that absorbance, and therefore film thickness, is a linear function of the number of CV cycles up to at least 60–70 cycles, indicating that the same amount of new polymer is produced in each cycle. With continued cycling, the polymerization solution eventually turns green, and electropolymerization ceases. The green color, which is removed by treatment of the solution with a base, is due to protonation of the pyrrole-type nitrogen atoms at the center of the porphyrin monomer in solution to generate the porphyrin dication, which does not electropolymerize. Electropolymerization can also be slowed or halted by addition of trifluoroacetic acid to the polymerization solution. It was found that the number of cycles required to

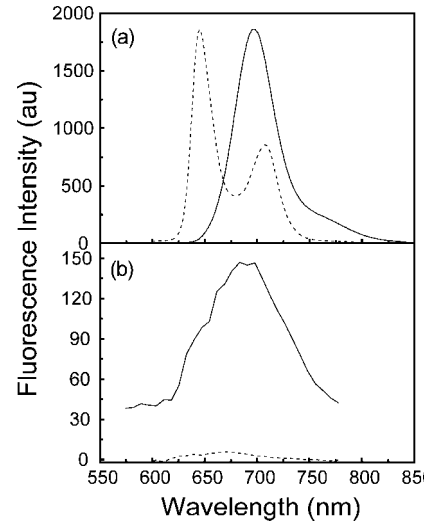

Figure 6. Fluorescence emission spectra with excitation at 420 nm. (a) Steady-state fluorescence emission spectra of monomer **1** (- - - -) and model compound **3** (———) in dichloromethane. (b) Time-resolved decay-associated spectra of the electropolymer on ITO in air. The time constants associated with the spectra are ~15 ps (———) and ~500 ps (- - - -).

bring about the protonation of the monomer was very dependent on the ratio of the electrode area to the solution volume.

The fluorescence emission spectra of **1** and **3** in dichloromethane with excitation at $\lambda = 420$ nm are shown in Figure 6a. Monomer **1** features peaks at 645 and 708 nm. Time-resolved measurements of the emission at 645 nm using the single-photon-timing technique gave data that were fitted as a single exponential decay with a lifetime of 8.94 ns ($\chi^2 = 1.16$). The emission of model porphyrin **3** consists of a broad band at 697 nm, with a shoulder at ~770 nm. Single-photon-timing experiments at 697 nm yielded a single exponential decay with $\tau = 5.98$ ns and $\chi^2 = 1.10$.

The emission of the polymer film on ITO was weak. It was investigated ($\lambda_{ex} = 420$ nm) using pulsed laser excitation and a streak camera, whose instrument response function in this experiment was 36 ps. Two slides of polymer film, one prepared with 50 CV cycles and the second with 100 cycles, were placed face-to-face for these measurements (total absorbance at 420 nm = 0.61), and the experiments were done in air. Figure 6b shows the decay-associated spectra obtained from analysis of these data. The film shows a broad emission with a maximum at about 680 nm, similar to that observed for model compound **3**. The fitting gave two lifetimes: a major component of ~15 ps and a very minor component of ~500 ps.

The excited singlet state of the polymer has a much shorter lifetime than those of **1** and **3**. This lifetime could be an inherent property of the polymer chromophores, but could also result from processes such as quenching by energy transfer within the polymer followed by charge injection into the ITO, electron transfer quenching within the polymer, or energy transfer to trap sites within the polymer followed by rapid deactivation. The energy of the porphyrin first excited singlet state of the polymer, estimated from the absorbance and emission spectra, is ~1.84 eV, whereas the cyclic voltammetry yields an estimate for the energy of a charge-separated state consisting of a porphyrin radical anion and

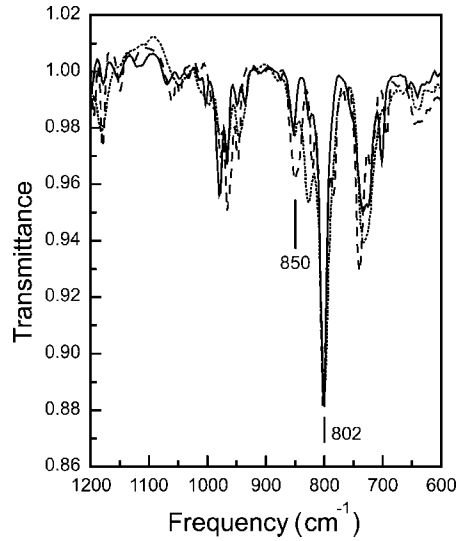

Figure 7. Fourier transform infrared spectra of monomer **1** (- - - -), model compound **3** (———), and electropolymerized **1** (80 CV cycles on gold) (• • • •). The spectra have been baseline corrected at a transmittance of 1.00 and normalized at the 802 cm^{-1} band. Note the differences in the 850 cm^{-1} region, as discussed in the text.

radical cation of ~1.97 eV. This suggests that rapid quenching via photoinduced electron transfer within the bulk of the polymer is unlikely unless trap sites of lower energy are available.

Mass Spectrometry. The polymer was extracted with pyridine, and the small amount of soluble material obtained was analyzed by MALDI-TOF mass spectrometry using a terthiophene matrix. The positive ion spectrum yielded major peaks at *m*/*z* 637.06, 1272.10, 1907.14, 2542.16, 3177.16, 3811.16, and 4445.12. The calculated exact mass for **1** ($C_{44}H_{39}N_5$) is 637.32. Each major peak in the mass spectrum is ~635 *m*/*z* greater than the previous peak. This is consistent with polymerization of **1**, with the loss of two hydrogen atoms per porphyrin monomer added to the growing chain.

Infrared Spectrometry. The Fourier transform infrared (FTIR) spectra of the polymer on gold (80 CV cycles) and of monomer **1** and model compound **3** were obtained using the attenuated total reflectance technique. Figure 7 shows the spectra in the 600–1200 cm^{-1} region. In general, the spectrum of the polymer resembles that of model **3** and differs appreciably from that of **1**. The region around 850 cm^{-1} is particularly illuminating. On the basis of experimental measurements and calculations, Zhang et al.[26] and Radziszewski et al.[27] have assigned a band at ~850 cm^{-1} to the meso C−H out-of-plane bending motion. Zhang et al. found that this band is significantly stronger in the spectrum of 5,10,15-triphenylporphyrin than in that of 5,10,15,20-tetraphenylporphyrin. In Figure 7, the spectra of the three substances have been normalized at 802 cm^{-1}, which has been assigned to out-of-plane bending of pyrrole N−H and C_β−H, hydrogen atoms, accompanied by a folding motion of the pyrrole rings.[26] It is clear from the figure that the 850 cm^{-1} absorption of monomer **1** is significantly stronger than those of **3** and the polymer, suggesting that the porphyrin rings in the polymer lack a *meso* hydrogen atom, as does model compound **3**.

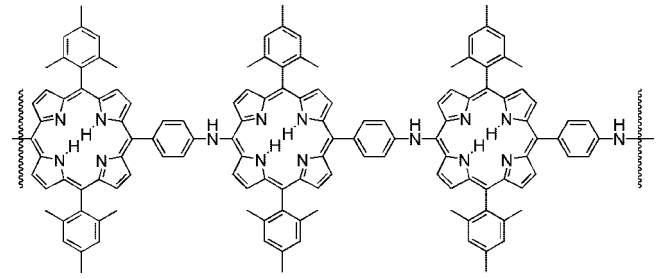

Figure 8. Proposed structure of electropolymerized **1**. The neutral form of the polymer is shown. Additional structures could be written for protonated and/or oxidized forms, as is the case with polyaniline.

Chemical Structure of the Polymer. Structural studies of the polymer are limited by the fact that the film is insoluble in common solvents. On the basis of the information delineated above, we propose that the polymer has the general structure indicated in Figure 8. The porphyrin units are linked together in a linear fashion via a bond between the aniline-type nitrogen atom and the meso position of the porphyrin macrocycle. There are several lines of evidence supporting this structure.

(i) The electropolymerization does not proceed with compound **2**, in which the meso position is blocked by a phenyl group, and related compounds.[7]

(ii) The mass spectral data demonstrate that the repeating unit is consistent with the proposed structure.

(iii) The UV–vis absorption spectrum of the film resembles that of model compound **3**, rather than that of the starting monomer.

(iv) The fluorescence emission spectrum of the polymer resembles that of model compound **3**, rather than that of **1**.

(v) The infrared spectrum indicates that the meso hydrogen atom of **1** has been lost in the polymer, as it has in **3**.

(vi) Anilines do not polymerize via the positions ortho or meta to the amino group.[13]

The polymerization mechanism is proposed to be related to that accepted for aniline.[28] Oxidation of the polymer on the electrode generates radical cations, as does oxidation of monomer in solution. It is possible to write resonance structures of the monomer radical cation in which the unpaired electron resides on the macrocycle meso position. Coupling of the two radicals and loss of two protons generates a new polymer unit. Consistent with this mechanism is the fact that as polymerization proceeds, the solution becomes acidic, and eventually the diprotonated dication of **1** is produced, halting the polymerization.

Figure 8 shows the neutral form of the polymer. Each subunit has three basic sites capable of protonation – the nitrogen at the meso position and two pyrrole-type nitrogen atoms. In addition, the polymer has various oxidation states associated with it. Thus, protonation and oxidation are expected to generate a number of different structures with different conductivities and UV–vis absorption characteris-

(26) Zhang, Y. H.; Ruan, W. J.; Li, Z. Y.; Wu, Y.; Zheng, J. Y. *Chem. Phys.* **2005**, *315*, 201–213.

(27) Radziszewski, J. G.; Nepras, M.; Balaji, V.; Waluk, J.; Vogel, E.; Michl, J. *J. Phys. Chem.* **1995**, *99*, 14254–14260.

(28) Syed, A. A.; Dinesan, M. K. *Talanta* **1991**, *38*, 815–837.

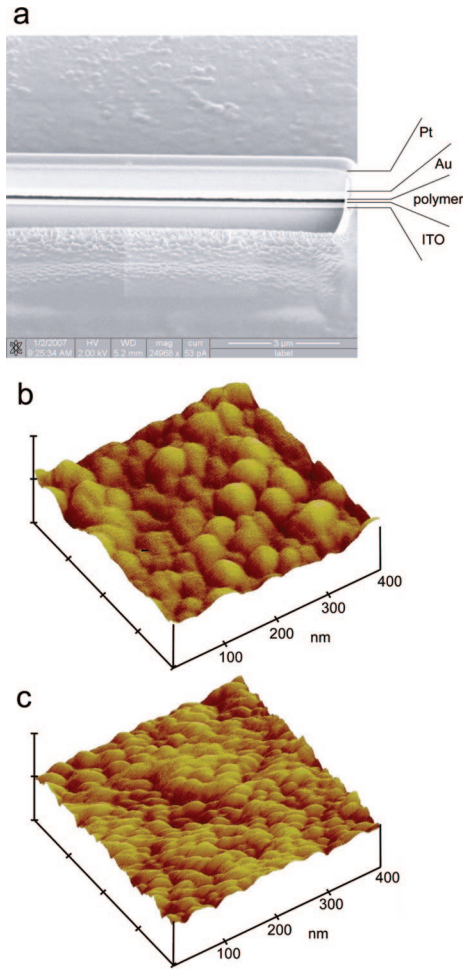

Figure 9. (a) Scanning electron microscopy image of electropolymerized **1** on ITO (absorbance of 0.78 at 428 nm). The polymer film was protected with sputtered layers of gold followed by platinum and then cut at the normal to the surface with a focused ion beam prior to imaging with SEM. The dark line indicates the polymer film in cross-section. The horizontal scale bar is 3 μm. (b) Tapping mode AFM image of the surface of polymerized **1** on ITO. The scale in the vertical direction is 25 nm per division. (c) Tapping mode AFM image of the surface of bare ITO. The scale in the vertical direction is 25 nm per division.

tics, as is the case with polyaniline. Although it is possible to write resonance forms of some of these structures with π-electron delocalization along the polymer backbone, à la polyaniline, the amount of delocalization will be reduced somewhat by the fact that the phenyl ring bearing the nitrogen atom is not coplanar with the plane of the porphyrin macrocycle because of steric hindrance.[29]

Morphology of the Film. The thickness and general morphology of the film were investigated. For these studies, polymer films were grown on an ITO electrode and coated with a sputtered layer of gold. A platinum layer was then applied in a focused ion beam (FIB) system. The metal layers served to both protect the polymer and provide contrast for imaging. Next, the FIB was used to cut cross-sections through the film. A scanning electron microscope (SEM) within the FIB apparatus was used to image the cut area. Typical results are shown in Figure 9a. The polymer film shows as a dark line. From this image and others we have taken, it is apparent

(29) Dirks, J. W.; Underwood, G.; Matheson, J. C.; Gust, D. *J. Org. Chem.* **1979**, *44*, 2551–2555.

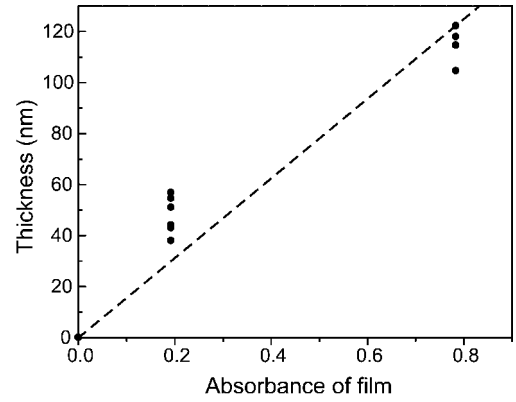

Figure 10. Plot of the absorbance of electropolymerized films of **1** at the Soret maximum as a function of the thickness as determined by the method illustrated in Figure 9. The data points are multiple thickness estimates obtained for slides with average UV–vis absorbances of 0.20 and 0.78. Absorbance of the ITO substrate was corrected to 0.0 in the absence of polymer. The data suggest that the absorbance is nearly, but not completely, linear with the number of cycles. The dashed line gives a slope of 15.5 nm per 0.10 absorbance unit, allowing a rough estimate of film thickness on the basis of the absorbance.

that on the scale of the image, the film is nearly uniform in thickness and relatively smooth. This evenness is consistent with the UV–vis spectra of the films. Properly prepared substrates yield films with uniform light absorbance characteristics throughout the film area. Two samples with different film thicknesses (different numbers of CV cycles) were prepared and studied using this technique. Figure 10 shows the film thickness measured from the SEM as a function of the absorbance at the Soret band maximum, taken from the UV–vis spectrum of the film before metal coating. Considering that the absorbance of an ITO slide at this wavelength is essentially 0, it is clear that the film absorbance is a nearly linear function of the thickness, within experimental error. The deviation from linearity is likely related to the fact that the UV–vis spectrum undergoes small shifts in wavelength maxima as the film grows thicker (vide supra), indicating small changes in morphology as the length of the polymer chains increases. Figure 10 allows rough estimation of film thickness on the basis of the absorption spectrum; a change in absorbance of 0.10 units at the Soret band corresponds to a ~15 nm thickness change. Growing films with a thickness of ~150 nm and an absorbance in the Soret region of 1.0 is not difficult.

Images b and c in Figure 9 show tapping-mode AFM images of the polymer film and a bare ITO substrate, respectively. The porphyrin forms a smooth layer that conforms to the irregularities of the underlying ITO, with no obvious defects at this scale. The difference in feature size between images b and c suggests that some of the smaller features on ITO are smoothed and obliterated as the film grows. This is consistent with a film growth rate perpendicular to the underlying local electrode surface, which is constant over all regions of the surface.

Conclusions

Porphyrin **1** readily undergoes oxidative electropolymerization to yield a conducting polymer. Various lines of evidence indicate that the polymer is linear, and made up of

repeating porphyrin units joined via the nitrogen atom of the aminophenyl group at the 5-position and the macrocycle carbon atom at the 15-position. Oxidation of the resulting film (0.85 V vs SCE) occurs more readily than reduction (−1.12 V vs SCE). The fact that the absorbance of the film, and therefore the thickness, increase linearly with the number of CV cycles up to a large number of cycles suggests that the film is a good hole conductor, although actual transport measurements have not yet been performed. The absorption and emission spectra of the polymer are similar to those of model compound **3**, except for significant broadening in the polymer. Thus, the porphyrin macrocycle is intact in the film. Light absorption by the film covers the entire visible spectral region. The first excited singlet state of the porphyrin moiety in the film on a conducting substrate has a much shorter lifetime (15 ps) than that of the model monomer, but the cause of this is not known. Migration of excitation within the film and electron transfer within the film and/or involving the conducting substrate may play roles in this apparent quenching. The electrical and optical properties of this film, coupled with the fact that it is simple to prepare on electrode surfaces, suggest that the polymer may prove useful as a component of solar-energy conversion devices, sensors, and catalysts.

Experimental Section

Electrochemistry. The voltammetric characterization of the redox process for the porphyrins was performed with a CH 600C potentiostat-galvanostat (CH Instruments) using a Pt disk working electrode of 0.021 cm^2 and a Pt counter electrode in a conventional three-electrode cell. Indium tin oxide (ITO) electrodes (Delta Technologies) with a nominal resistance of 8–12 Ω/■, gold, and glassy carbon electrodes were also used as working electrodes. When ITO electrodes were used, the counter electrode was isolated from the monomer solution by a glass frit in order to avoid interference with the redox reactions occurring at the working electrode. Electrochemical studies were carried out in acetonitrile deoxygenated by bubbling with nitrogen, with 0.10 M tetra-*n*-butylammonium hexafluorophosphate as the supporting electrolyte. A freshly prepared Ag/AgCl quasi-reference electrode was used. The working electrode was cleaned between experiments by polishing with 0.3 μm alumina paste followed by solvent rinses. After each voltammetric experiment, ferrocene was added, and the potential axis was calibrated against the formal potential for the ferrocenium/ferrocene redox couple.

Spectroscopy. Absorption spectra were measured on a Shimadzu UV-3101PC UV–vis−NIR spectrometer. Steady-state fluorescence spectra were measured using a Photon Technology International MP-1 spectrometer and corrected for detection system response. Excitation was provided by a 75 W xenon-arc lamp and single grating monochromator. Fluorescence was detected 90° to the excitation beam via a single grating monochromator and an R928 photomultiplier tube having S-20 spectral response and operating in the single photon counting mode. Fluorescence decay measurements on solutions of **1** and **2** were performed on $\sim 1 \times 10^{-5}$ M solutions by the single photon timing method. The excitation source was a titanium sapphire (Ti:S) laser (Spectra Physics, Millennia-pumped Tsunami) with a 130 fs pulse duration operating at 80 MHz. The laser output was sent through a frequency doubler and pulse selector (Spectra Physics model 3980) to obtain 420 nm pulses at 4 MHz. Fluorescence emission was detected at the magic angle using a double grating monochromator (Jobin Yvon Gemini-180) and a microchannel plate photomultiplier tube (Hamamatsu R3809U-50). The instrument response function was 35–45 ps as verified by scattering by a solution of nondairy coffee creamer in water. The average energy per pulse was measured to be 6.8 nJ. The spectrometer was controlled by software based on the LabView (National Instruments) programming language and data acquisition was done using a single photon counting card (Becker-Hickl, SPC-830). Data were analyzed using a sum of exponentials decay model with the ASUFIT program that was written in-house using MATLab software (Math Works).

The time versus wavelength fluorescence intensity surfaces for the film were recorded on a system consisting of an ultrafast laser and a streak camera. The 130 fs light pulses at 840 nm were generated by a mode-locked titanium:sapphire (Ti:S) laser (Mira 900, Coherent Laser) pumped by a frequency-doubled Nd:YVO**4** laser (44% from an 18 W Verdi, Coherent Laser). The repetition rate of the Ti:S laser was reduced to 4.75 MHz by a pulse picker (Model 9200, Coherent Laser). The excitation light was frequency doubled to 420 nm and focused on the sample, which consisted of two polymer-sensitized ITO electrodes arranged in a face-to-face configuration. This arrangement was employed to increase the amount of material available for excitation.

Fluorescence was collected 90° to the excitation beam and focused on the entrance slit of a Chromex 250IS spectrograph, which was coupled to a Hamamatsu C5680 streak camera with an M5675 synchroscan sweep unit. The streak images were recorded on a Hamamatsu C4742 CCD camera. The full width at half-maximum of the overall time response of this system was 36 ps when measured on a 2 ns time scale (1024 pixels). The spectral resolution was 0.25 nm/pixel in the spectral range of 550−800 nm. Global analysis was performed using the ASUFIT program, which was programmed in-house using MATLab software (Math Works). The 1024 kinetic traces were binned, resulting in a spectral resolution of 5 nm. A Gaussian-shaped instrument response function was used in the fitting.

For infrared spectra, a Bruker IFS 66V/S Fourier transform infrared spectrometer was used with an attenuated total reflectance sample holder and an evacuated sample chamber. The monomer and model compound samples were deposited directly on the ATR from solution in dichloromethane, whereas the polymer sample was electropolymerized on a gold substrate, which was then clamped against the ATR.

Mass Spectrometry. Mass spectrometry was performed by the MALDI-TOF method using a Voyager DE STR from Applied Biosystems. The spectrometer incorporates a nitrogen laser producing 337 nm pulses with a duration of 3 ns at a frequency of either 3 or 20 Hz. A terthiophene matrix was employed.

Thickness Measurements. Samples of polymer were prepared by electropolymerization of **1** on ITO-covered glass. After obtaining the absorption spectra, the samples were protected by coating them with a sputtered layer of gold. They were then placed in a focused ion beam (FIB) system, the Nova 200 Dual Beam SEM/FIB manufactured by the FEI Company. Just prior to cutting the cross-sections, an additional protecting layer of platinum was deposited using the FIB. The FIB was then used to cut cross-sections of the samples, and the cross-sections were imaged using the integral scanning electron microscope. The SEM images were used to estimate the thickness of

the polymer layers, correcting for parallax resulting from the angle between the cut face of the polymer and the SEM.

Synthesis. Synthetic details appear in the Supporting Information

Acknowledgment. This work was supported by a Grant from the U.S. Department of Energy (DE-FG02-03ER15393). We gratefully acknowledge the use of facilities within the LeRoy Eyring Center for Solid State Science at Arizona State University. The streak camera fluorescence spectrometer was funded by NSF Grant CHE-0541835.

Supporting Information Available: Synthetic details for preparation of **1**, precursors, and model compounds (PDF). This material is available free of charge via the Internet at http://pubs.acs.org.

CM7022955